A Basic Research on the Improvement of Propulsion Maneuvering System and the Automatic Motion Control of SHINKAI6500

Takuya SHIMURA, Yasutaka AMITANI, Takao SAWA and Yoshitaka WATANABE

Japan Marine Science and Technology Center (JAMSTEC)
2-15, Natsushima-cho, Yokosuka, 237-0061, Japan

***Abstract*- SHINKAI 6500, a manned-submersible possessed by JAMSTEC (Japan Marine Science and Technology Center) has made great results for 10 years since it started operation. Recently the sophisticated ship maneuvering technology has been required such as hovering under irregular current or moving along obstacles like a wall. The response of thrusters equipped with SHINKAI6500 in present is not so fast because they were mainly designed to move the vehicle straightly and to reduce the radiation noise. Moreover they are manipulated individually, so it is difficult to do operations as mentioned and depends on operator's skills. Then this study was carried out as a basic research to develop the propulsion maneuvering system that enables quick motion and advanced position attitude control using multiple rapid response thrusters and to reduce the burden of operators by using automatic control with those thrusters.**

First in this study, to improve the response of thrusters, experimental thrusters were developed and real sea test at which they were equipped with SHINKAI6500 temporarily was executed. It was ensured that the thrust and response of the thrusters are adequate and they can sufficiently improve the motion response of the vehicle. Secondly in order to get more precise positioning compared with conventional acoustic positioning system, the test to use Doppler sonar as a positioning sensor by measuring the relative velocity to the bottom was executed. It was verified that it is possible to get enough accuracy. At last, the test of station-keeping control on the forward-backward direction was tried as a basic test that the vehicle motion was controlled by automatic control. In this test, "optimum control" of modern control algorithm was adopted as an algorithm generally used, and in addition, the "Ossman's adaptive control" algorithm was used to better position control accuracy. The results shows that it is possible to keep position at the high accuracy that 2σ is 4~5mm.

I. INTRODUCTION

The Japan Marine Science and Technology Center's SHINKAI6500 is a deep-sea manned research submersible which boasts the greatest operational depth in the world. Since its launch in 1989, it has made great contributions to the center's research programs. In recent years, however, demands for more sophisticated maneuvering capabilities, such as hovering in irregular currents and moving along a wall or a similar underwater object, have arisen.

Since the thrusters currently mounted on the SHINKAI6500 were designed with an emphasis on quiet operation and straight-line cruising performance, their start-up response is rather slow. Moreover, as these thrusters are operated individually, sophisticated maneuvering is difficult, and complex maneuvers, such as those mentioned above, are at present left to the operator's skills.

Against this background, this study was conducted to lay a foundation for the development of an automatic propulsion control system based on multiple fast-response thrusters and a Doppler sonar or some other positioning sensor as a means of reducing the burden on the operator by enabling swift vehicle movement and advanced position and attitude control.

First, with a view to improving thruster response, experimental thrusters were produced and temporarily mounted on the SHINKAI6500, with motion experiments conducted to establish the adequacy of their thrust force and response performance and assess the motion response of the submersible when powered by the experimental thrusters in comparison with the current thrusters.

Next, a Doppler sonar was used as a positioning sensor, and its positioning accuracy was compared with that of a conventional acoustic positioning device to verify its suitability for position control use.

Lastly, a position-keeping control experiment in surge direction was conducted as a basic investigation into the automatic motion control of the submersible. Although numerous research papers have been published on the position and attitude control of underwater vehicles, most only discuss simulation results, with a small number backed up with model experiments, and experiments involving a real vehicle are rare. With this in mind, real-vehicle hovering experiments were conducted using optimal control theory and Ossman's adaptive control theory, with hovering control accuracy measured in both cases.

II. EXPERIMENTAL THRUSTER

As shown in Fig. 1, the SHINKAI6500 is currently equipped with a large-diameter main propeller, a bow thruster and two vertical thrusters. With a limit set on the

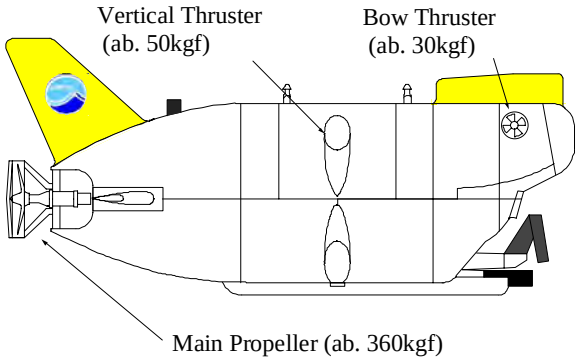

Fig.1 Thrusters equipped with SHINKAI6500

Fig. 2 Experimental Thruster

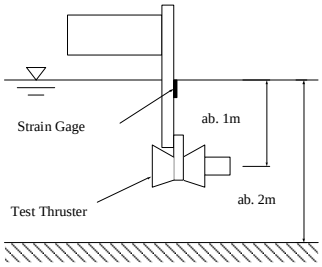

Fig.3 Equipment Layout of Thruster Tank Experiment

start-up speed of the propulsion system to protect the inverter circuits the main propeller takes as long as 13 seconds to reach full speed, while the vertical and bow thrusters both need 11 seconds. The main propeller can be swung through ± 85°, but swinging speed is also low, approx. 10° per second. Such slow thruster response, combined with individual manual thruster operation, makes sophisticated vehicle maneuvering very difficult - as has been mentioned in the INTRODUCTION.

As a first step towards improving the response of the propulsion system, two experimental thrusters were produced. As well as being capable of fast response, the motors that drive these thrusters must be able to operate at DC 108V under 6500-m deep-sea high pressure conditions

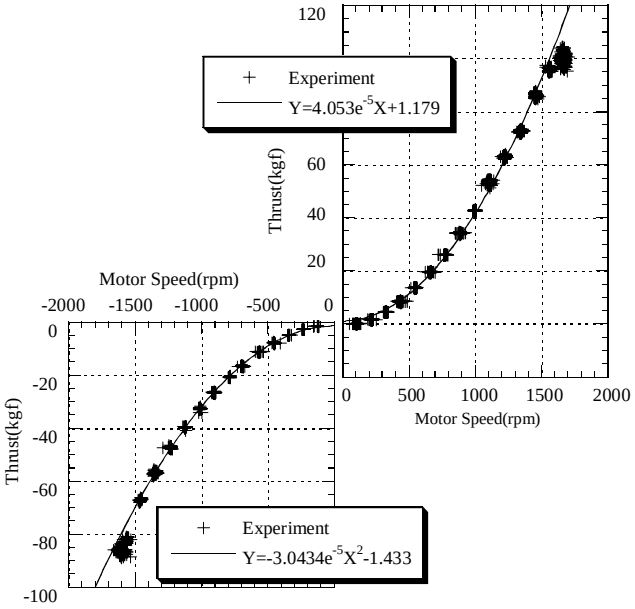

Fig. 4 Steady State Characteristics of Experimental Thruster

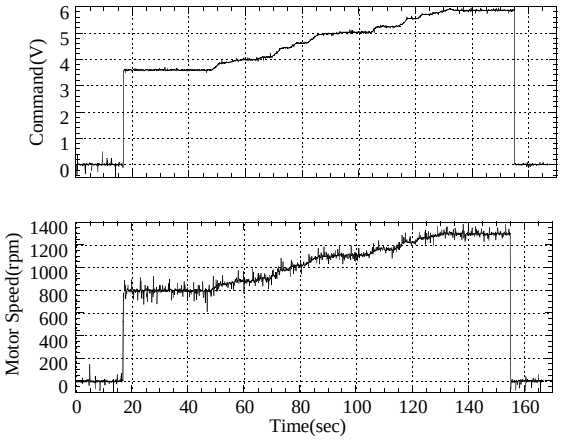

Fig. 5 Step Response of Experimental Thruster

to be used for SHINKAI6500. In light of these requirements, Kollmorgen Co.'s oil-immersed brushless motor Model S-404-E-21 was chosen. The most desirable qualities of the propellers, on the other hand, were high efficiency in the low speed region and minimal thrust loss when turning in the reverse direction, leading to the selection of Innerspace Co.'s ducted propeller Model 1002. Fig. 2 shows the experimental thruster that consists of this motor and propeller.

To determine whether the produced thrusters had the required characteristics, a water tank experiment was conducted to measure their thrust force as shown in Fig. 3. The results are shown in Fig. 4. As can be seen from this, the

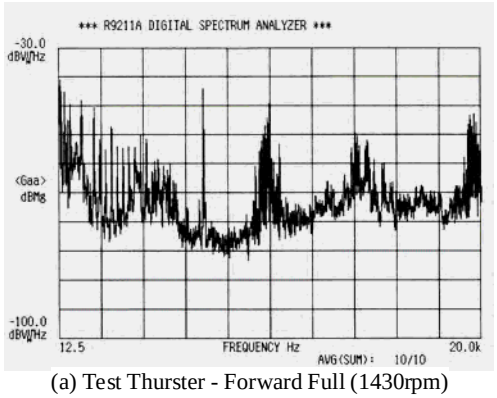

(a) Test Thurster - Forward Full (1430rpm)

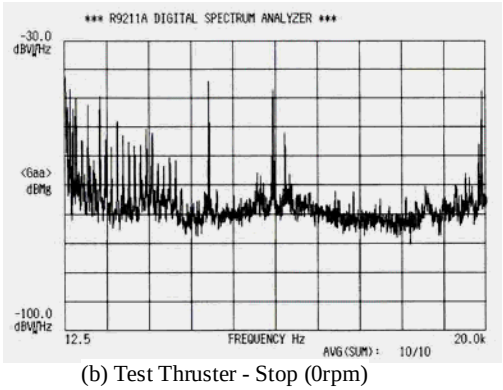

(b) Test Thruster - Stop (0rpm)

Fig. 6 Experimental Thruster Noise

thrusters are able to generate a thrust force of about 135 kgf at the maximum rotational speed of 1750 rpm, with the backward direction thrust force as high as 90% of the forward direction thrust force. These results demonstrate that they are indeed very high-efficiency thrusters.

Regarding the crucial start-up response performance, the results of an ocean field experiment conducted at a depth of 3000 m are shown in Fig. 5. The upper graph represents the rotational-speed command signal, while the lower graph represents the actual rotational speed of the thrusters. As can be seen from these results, the thrusters respond to the command with little delay, even to a step-input-like command, thus exhibiting excellent response characteristics.

As radiation noise from thrusters should not interfere with the operation of the acoustic equipments mounted onboard the SHINKAI6500 if they are installed practically in the future, the radiation noise of the experimental thrusters was measured.

In concrete terms, the net increases in noise levels due to the operation of the thrusters were measured during the ocean field experiment to be discussed later using a hydrophone installed at the location shown in Fig. 9. Fig. 6 shows the FFT analysis results of the measurement data. The lower graph represents the noise levels measured with the thrusters turned off, while the upper graph represents the noise levels measured with the thrusters operational at 1430 rpm. A comparison of the two graphs revealed that there was some noise generation at around 14 kHz. However, this does not seem to pose a problem, as the frequency band concerned will not affect the acoustic equipment currently in use.

III. POSITIONING BY DOPPLER SONAR

The SHINKAI6500 is equipped with an acoustic positioning system to keep track of its approximate position. However, as the depth increases to several thousand meters, the positioning rate falls to at best four to eight seconds, and the positioning accuracy deteriorates to several meters even with LBL positioning. For this reason, there have been calls for a positioning sensor with a greater positioning accuracy and faster positioning rate to provide the vehicle with more detailed information about its position. In the area of underwater vehicle control as will be discussed later, the current sensor is inadequate for automatic hovering control use in terms of both accuracy and positioning rate, and this has been a major problem.

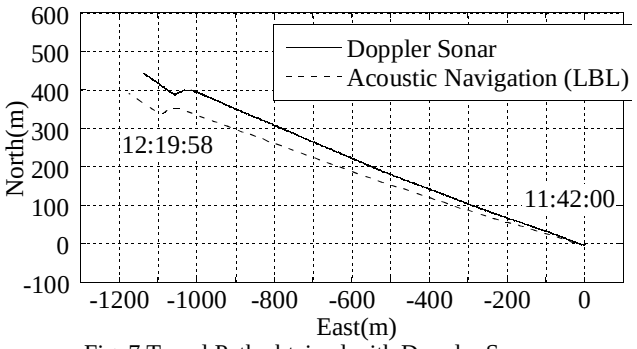

Fig. 7 Travel Path obtained with Doppler Sonar

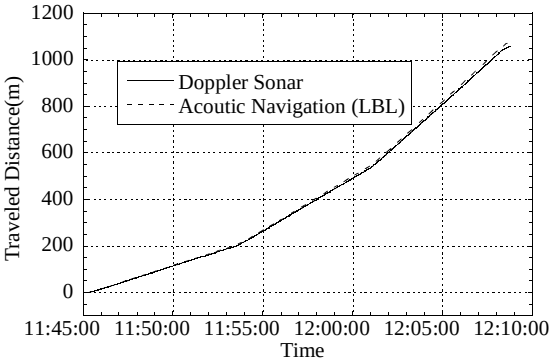

Fig. 8 Comparison of Measured Travel Distances

With this in mind, this study attempted to measure the velocity to the bottom of the vehicle using a Doppler sonar mounted on the bottom of the vehicle, with the relative changes in position obtained by integrating the velocity to the bottom in real-time. Although this kind of approach has been investigated before, there appears to have been no instance of a sensor being tested by actually mounting it on an underwater vehicle. For this reason, the experiment sought to establish whether a Doppler sonar could be used as a position sensor.

The Doppler sonar used in the experiment was RD Instruments Co.'s Workhorse DVL, which had the following specifications: frequency 300 kHz; range 1- 200 m; and accuracy (standard deviation) of velocity to the bottom measurement 3 mm/s at a steady-state speed of 1.0m/s.

Fig. 7 compares the travel paths of the submersible after 25 minutes of straight-line cruising as obtained with a Doppler sonar and an acoustic positioning system. In this test, the Doppler sonar exhibited a poorer accuracy than the acoustic positioning system, producing a rather distorted travel path, as its built-in compass was a fluxgate type not so accurate as a mechanical gyro mounted onboard the submersible.

To avoid this heading error, only forward direction travel distances were plotted in Fig. 8 in order to ensure that the relative positioning using a Doppler sonar does not give rise to a large drift due to integration. In contrast, an acoustic positioning system is immune to drift, although it may still be subject to scattering. For this reason, the measurement result obtained with the acoustic positioning system (1076.7 m) was assumed to be correct. Given that the measurement result obtained with the Doppler sonar was 1058.5 m, there was only a 2% error.

These results show that a Doppler sonar is reasonably well suited for positioning use as long as integration time is kept sufficiently short to prevent diversion from occurring, i.e. around 10 to 20 minutes. From here on, therefore, all measurement results will be based on a Doppler sonar.

IV. MOTION TESTS VIA MANUAL OPERATION

Next, ocean field experiments were conducted by manually operating experimental thrusters to measure vehicle motions and drag coefficients, with the characteristics of vehicle motion when powered by the experimental thrusters compared with those of vehicle motion when powered by the existing thrusters.

As shown in Fig. 9, the experimental thrusters and Doppler sonar were mounted on the SHINKAI6500 on an

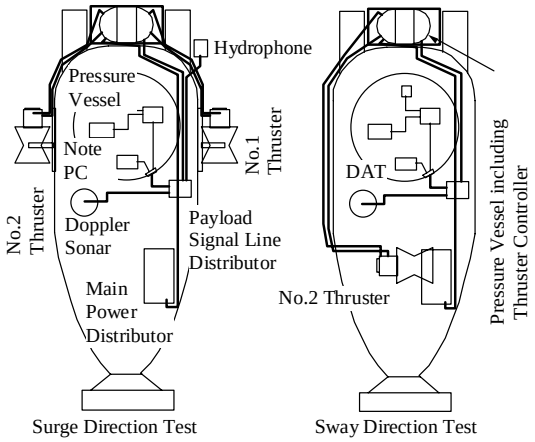

Fig. 9 Layout of Test Equipments

experimental basis, and the following tests were conducted: the measurement of motions in forward direction with an experimental thruster mounted on each side of the vehicle; and the measurement of swaying and yawing motions with one of the experimental thrusters mounted sideways on top of the stern and operated simultaneously with the existing bow thruster.

A. Motion tests in forward direction

Fig. 10 shows the results of forward motion tests. The upper graph represents the rotational speeds of the experimental thrusters, while the lower graph represents the velocity to the bottom of the submersible. As the thrusters were powered from the power outlets for payloads, the rotational speed was limited to 1430 rpm, which corresponded to the maximum allowable current for payload.

Fig. 11 shows graphs that compare the motions of the submersible when it is powered by the experimental thrusters and the existing main propeller. A similar thrust force was applied in both cases. As the graph for the main propeller shows a wobble a few dozen seconds into start-up, it is somewhat poor as reference data. Nevertheless, it is does show that there was a marked delay between the times the propeller started turning and the submersible started

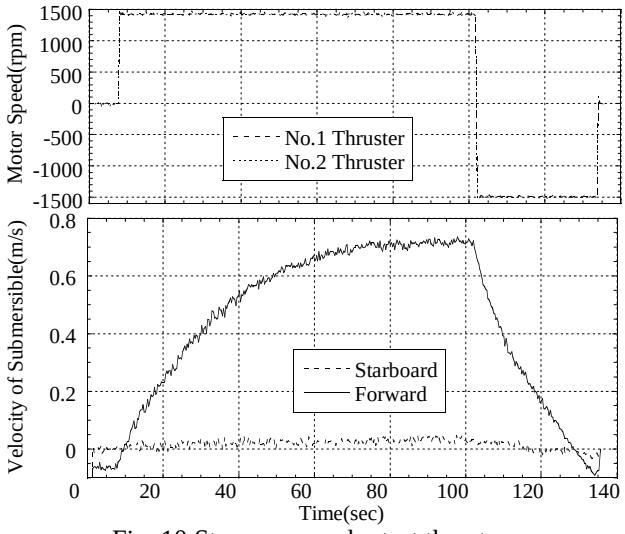

Fig. 10 Step response by test thruster

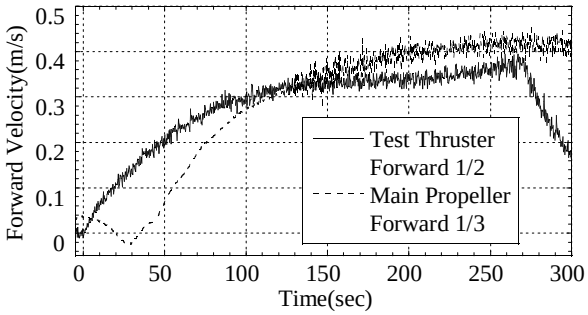

Fig. 11 Comparison of Step Responses

moving. In contrast, start-up was very rapid with experimental thrusters, so much so that acceleration was physically felt as the submersible started moving.

From this, it is evident that the use of the experimental thrusters would greatly improve the response speed of the submersible with regard to starting, stopping, etc.

The forward direction drag coefficient of the submersible was calculated to be about 0.25 on a $\nabla^{2/3}$ base.

B. Swaying and yawing motion tests

Swaying and yawing motion tests were conducted as described at the beginning of this section. In both tests, the submersible was manually operated using the experimental thruster mounted sideways on top of the stern in such a manner that its thrust force would balance with that of the bow thruster. Figs. 12 and 13 show the motion paths of the submersible under these tests.

In these tests, the submersible was moved several times, and the steady state velocity or angular velocity was measured each time, with drag coefficients also calculated. On average, the drag coefficient was about 4.1 for swaying motion and 0.51 for yawing motion, although some scattering was observed with the latter.

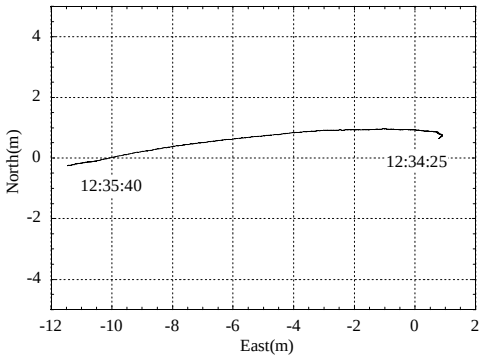

Fig. 12 Path of Submersible under Swaying Motion Test

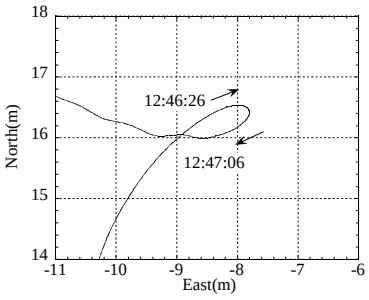

Fig. 13 Path of Submersible under Yawing Motion Test

V. POSITION-KEEPING TEST USING AUTOMATIC COTROL

In this study, a position-keeping control experiment in surge direction was also conducted using experimental thrusters and a Doppler sonar as a basic investigation into the automatic position and attitude control of the submersible. This section summarizes the results of the experiment.

A. Equation of motion of submersible

With the longitudinal axis of the submersible defined as an x-axis whose arrow points in the forward direction, its one-dimensional equation of motion for the surge direction is expressed as follows:

$$m\ddot{x}(t) + c\dot{x}(t) = f(t) \tag{5.1}$$

where m is the sum of the mass of the submersible and added mass; c is a linearized damping coefficient; and f is an external force.

As the adaptive control algorithm to be discussed later is a discrete control algorithm, (5.1) is discretized by central difference to produce (5.2), which is in the form of a DARMA model.

$$x(t+1) = \left(\frac{m}{\Delta^2} + \frac{c}{2\Delta}\right)^{-1}\left[\frac{2m}{\Delta^2}x(t) + \left(\frac{c}{2\Delta} - \frac{m}{\Delta^2}\right)x(t-1) + f(t)\right] \tag{5.2}$$

where Δ is sampling time.

B. Control Algorithm

Generally speaking, preferred algorithms for the position control of surface vessels and underwater vehicles are PID control algorithms based on classic control theory and optimal control algorithms based on modern control theory, and these can be regarded as theoretically well-established algorithms.

However, as these algorithms are linear control algorithms, they require the linearization of its equation of motion. For this reason, factors such as the nonlinearity of fluid forces, nonlinearity due to a delay in the thrust response of a thruster, high-order coupled terms, and the dynamics of trapped fluid are ignored, and this is believed to be a cause of inferior control performance. In the case of PID control, which deals with single input single output systems, further degradation in control performance may occur, as couplings between different modes of motion are ignored.

Of the commonly used control algorithms, an optimal control algorithm was tested in this study, followed by an adaptive control algorithm designed to improve control performance by compensating omitted dynamics as mentioned above.

As is well known, adaptive control theory estimates system parameters from output and input signals and adjusts the feedback gain in real-time using those estimated parameters to deal with unknown dynamics and variations in the system.

The adaptive control algorithm employed in this study was one devised by Ossman, which will be discussed in detail in the following subsection.

C. *Ossman's adaptive control algorithm*[1)]

Generally speaking, a self-tuning controller (STC) in adaptive control requires a control force with the characteristics of persistent excitation to be input into the estimation mechanism as a condition for the convergence of estimated parameters on the true values and ultimately the stability of the system. A persistent excitation input is an input that has all frequency components, and is therefore not a realistic option in dynamic system control. To overcome this problem, Ossman devised a MIMO (multiple input multiple output) linear discrete adaptive regulator that did not require persistent excitation. A concrete explanation of this regulator follows.

Firstly, a MIMO linear discrete system is expressed in the form of a DARMA model.

$$\boldsymbol{y}(k) = -\sum_{j=1}^{p}\boldsymbol{A}_j\boldsymbol{y}(k-j) + \sum_{j=1}^{q}\boldsymbol{B}_j\boldsymbol{u}(k-j) = \boldsymbol{\theta}^T\boldsymbol{\varphi}(k-1) \tag{5.3}$$

$$\boldsymbol{\theta}^T = \left[-\boldsymbol{A}_1, \cdots, -\boldsymbol{A}_p, \boldsymbol{B}_1, \cdots, \boldsymbol{B}_q\right], \quad \boldsymbol{\varphi}(k-1) = \begin{bmatrix} \boldsymbol{y}(k-1) \\ \vdots \\ \boldsymbol{y}(k-p) \\ \boldsymbol{u}(k-1) \\ \vdots \\ \boldsymbol{u}(k-q) \end{bmatrix}$$

where $\boldsymbol{y}$ and $\boldsymbol{u}$ are system output and input vectors; $\boldsymbol{\theta}$ is a matrix composed of system parameters; and $\boldsymbol{\varphi}$ is a regression vector composed of past input and output vectors.

The value of $\boldsymbol{\theta}$, which represents the control system, is estimated from input and output information via the following estimation mechanism:

$$\begin{aligned} \boldsymbol{\theta}(k) &= \boldsymbol{\theta}(k-1) - \boldsymbol{P}(k-1)\boldsymbol{f}(\boldsymbol{\theta}(k-1)) \\ &\quad + \frac{\boldsymbol{P}(k-1)\boldsymbol{\varphi}(k-1)}{\eta_{k-1}^2 + \boldsymbol{\varphi}(k-1)^T\boldsymbol{P}(k-1)\boldsymbol{\varphi}(k-1)} \\ &\quad \times [\boldsymbol{y}^T(k) - \boldsymbol{\varphi}^T(k-1)\boldsymbol{\theta}(k-1)] \\ \boldsymbol{P}(k) &= \boldsymbol{P}(k-1) - \frac{\boldsymbol{P}(k-1)\boldsymbol{\varphi}(k-1)\boldsymbol{\varphi}(k-1)^T\boldsymbol{P}(k-1)}{\eta_{k-1}^2 + \boldsymbol{\varphi}(k-1)^T\boldsymbol{P}(k-1)\boldsymbol{\varphi}(k-1)} \\ 0 < \boldsymbol{P}(0) &= \boldsymbol{P}(0)^T < 2\boldsymbol{I} \\ f_{ij}(k-1) &= \begin{cases} \theta_{ij}(k-1) - \theta_{ij}^{\max}, \text{when } \theta_{ij}(k-1) > \theta_{ij}^{\max} \\ \theta_{ij}(k-1) - \theta_{ij}^{\min}, \text{when } \theta_{ij}(k-1) < \theta_{ij}^{\min} \\ 0, \quad \text{when } \theta_{ij} \in [\theta_{ij}^{\max}, \theta_{ij}^{\min}] \end{cases} \end{aligned} \tag{5.4}$$

The estimation mechanism uses a modified recursive least squares algorithm which aims to cause parameter vector $\boldsymbol{\theta}$ to converge within the predetermined range $[\boldsymbol{\theta}_{\max}, \boldsymbol{\theta}_{\min}]$, instead of exactly on the true value, to ensure its convergence on a value that is appropriate in light of the obtained input and output information.

A state space model in the form of (5.5) is then developed from the estimated value of $\boldsymbol{\theta}$, denoted as $\boldsymbol{\theta}(k)$.

$$\begin{aligned} \boldsymbol{x}(k+1) &= \boldsymbol{F}(k)\boldsymbol{x}(k) + \boldsymbol{G}(k)\boldsymbol{u}(k) \\ \boldsymbol{y}(k) &= \boldsymbol{H}\boldsymbol{x}(k) \end{aligned} \tag{5.5}$$

$$\boldsymbol{F}(k) = \begin{bmatrix} -\boldsymbol{A}(k)_1 & \boldsymbol{I} & & & \\ -\boldsymbol{A}(k)_2 & & \boldsymbol{I} & & \\ \vdots & & & \ddots & \\ -\boldsymbol{A}(k)_{n-1} & & & & \boldsymbol{I} \\ -\boldsymbol{A}(k)_n & \boldsymbol{0} & \boldsymbol{0} & \boldsymbol{0} & \boldsymbol{0} \end{bmatrix}, \quad \boldsymbol{G}(k) = \begin{bmatrix} \boldsymbol{B}(k)_1 \\ \boldsymbol{B}(k)_2 \\ \vdots \\ \boldsymbol{B}(k)_{n-1} \\ \boldsymbol{B}(k)_n \end{bmatrix}$$

$$\boldsymbol{H} = [\boldsymbol{I} \cdots \boldsymbol{0}]$$

Based on (5.5), the feedback gain $\boldsymbol{L}(k)$ is determined using an LQ control law as follows:

$$\begin{aligned}
&\boldsymbol{u}(k) = -\boldsymbol{L}(k)\boldsymbol{x}(k) \\
&\boldsymbol{L}(k) = [\boldsymbol{G}(k)^T \boldsymbol{R}_k \boldsymbol{G}(k) + \boldsymbol{I}]^{-1} \boldsymbol{G}(k)^T \boldsymbol{R}_k \boldsymbol{F}(k) \\
&\boldsymbol{R}_{k+1} = \boldsymbol{Q} + \boldsymbol{L}(k)^T \boldsymbol{L}(k) \\
&\qquad + (\boldsymbol{F}(k) - \boldsymbol{G}(k)\boldsymbol{L}(k))^T \boldsymbol{R}_k (\boldsymbol{F}(k) - \boldsymbol{G}(k)\boldsymbol{L}(k))
\end{aligned} \tag{5.6}$$

In (5.6), the feedback gain is updated by solving a discrete Riccati equation step by step, alongside the estimation of parameters in (5.4). Here, $\boldsymbol{R}_k$ is the solution to the discrete Riccati equation, and $\boldsymbol{Q}$ is a weighting matrix for the state variables of the evaluation function.

Thus, the adaptive control algorithm is a combination of a parameter estimation mechanism, which takes the form of (5.4), and a control system, which takes the form of (5.5) and (5.6), and its overall stability, which is attributed to the conversion of the inputs and outputs to zero regardless of their initial states, has been theoretically proven by Ossman. As can be seen from (5.6), its control law is an LQ control law, the same as optimal control, and in this sense, adaptive control seems to offer better control performance through an adjustment of the feedback gain via parameter estimation.

The author et al. have applied this algorithm to the response control of an underwater elastic structure and have shown that it produces superior results to optimal control through a model experiment[2]. In that instance, adaptive control proved to be particularly effective in alleviating elastic deformation, while its application to a control problem involving the position-keeping of a rigid body also appeared promising. Against this background, this study adopted the same algorithm to carry out the position control of an underwater vehicle, which is a rigid body, in an attempt to improve control performance.

Notably, $\boldsymbol{y}(k)$ and $\boldsymbol{u}(k)$ in (5.3) become scalars here, as the study concerns one-dimensional control in the surge direction.

D. Setting of parameters

In adaptive control, the control system is built by substituting the discretized equation of motion (5.2) into (5.3) and subsequent equations.

In optimal control, on the other hand, control is started only after feedback gain $\boldsymbol{L}$ is determined. In concrete terms, $\boldsymbol{L}$ is first calculated by building a state space model similar to (5.5) from equation of motion (5.2) and solving discrete Riccati equation (5.6), and then control proceeds as $\boldsymbol{L}$ is fixed. This is equivalent to adaptive control minus a parameter estimation mechanism.

In this regard, the coefficients of (5.1) were set as follows: m=31. 5 tons, determined as the sum of the mass of the submersible (approx. 26.5 tons) and added mass, which was estimated[3] for the surge direction by assuming the shape of the vehicle body to be an ellipsoid; and $c = \frac{1}{2}\rho C_d \nabla^{\frac{2}{3}} \times 2$, where C_d=0.25 as was obtained in the previous section. The latter is equivalent to a linearization of intrinsically nonlinear fluid resistance, which takes the form $\frac{1}{2}\rho C_d \nabla^{\frac{2}{3}} \dot{x}(t)\left|\dot{x}(t)\right|$, at the point where $\dot{x}(t) = 1.0$.

The value of $\boldsymbol{\theta}$ obtained by substituting these values into (5.2) and further substituting this into (5.3) is named $\boldsymbol{\theta}_0$, and the values of $\boldsymbol{R}$ and $\boldsymbol{L}$ calculated from $\boldsymbol{\theta}_0$ are named $\boldsymbol{R}_0$ and $\boldsymbol{L}_0$, respectively. As these $\boldsymbol{\theta}_0$, $\boldsymbol{R}_0$ and $\boldsymbol{L}_0$ have been determined on the basis of the values of m and c mentioned above, they may be regarded as the "most accurate values foreseeable in advance".

In contrast, $\boldsymbol{L}$ is adjusted online through the estimation of parameter vector $\boldsymbol{\theta}$ in adaptive control, and this often gives rise to poor transient response due to large fluctuations in the estimated value of $\boldsymbol{\theta}$. For this reason, how to set the initial values of $\boldsymbol{\theta}$, $\boldsymbol{R}$ and $\boldsymbol{L}$ is a problem. The author et al. have shown that the use of $\boldsymbol{\theta}_0$, $\boldsymbol{R}_0$ and $\boldsymbol{L}_0$ mentioned above as initial values can sufficiently suppress the transient response observed at the initial stage of control[2]. This boils down to an attempt to mitigate the fluctuation of $\boldsymbol{\theta}$, $\boldsymbol{R}$ and $\boldsymbol{L}$ through the utilization of as much information available in advance, and the same approach was used in this study by adopting $\boldsymbol{\theta}_0$, $\boldsymbol{R}_0$ and $\boldsymbol{L}_0$ as initial values.

The convergence range of $\boldsymbol{\theta}$, $[\boldsymbol{\theta}_{\max}, \boldsymbol{\theta}_{\min}]$, was set as $\boldsymbol{\theta}_0 \pm 10\%$ in light of the fact that $\boldsymbol{\theta}_0$ represents the "most accurate value foreseeable in advance". The weighting matrix of an LQ control law, $\boldsymbol{Q}$, was set to $\boldsymbol{Q}$=1.0e$^6\boldsymbol{I}$, a value that will keep the thrust force of a thruster from exceeding the upper limit according to a linear simulation.

E. Experimental results

In the experiment, an initial deviation was introduced whereby position-keeping control was provided after moving the submersible a certain distance (e.g. 1 m) from an initial point to the target point.

Fig. 14 shows the results obtained from optimal control, while Fig. 15 shows those obtained from adaptive control. In both cases, the upper graphs represent the controlling force command to the thrusters, and the lower graphs represents relative displacement.

With both algorithms, the accuracy of position-keeping control in the neighborhood of the target point was about 4 mm in terms of 2σ, which is twice of the standard deviation, and this shows that position-keeping control is sufficiently accurate. The steady-state deviation, ε, was 16 mm for optimal control and 13 mm for adaptive control, and therefore adaptive control was slightly more effective. The reason why there was not much difference between the results of adaptive control and optimal control is because the experiment was about one-dimensional control of a rigid body, so that omitted dynamics as mentioned before did not have a major impact.

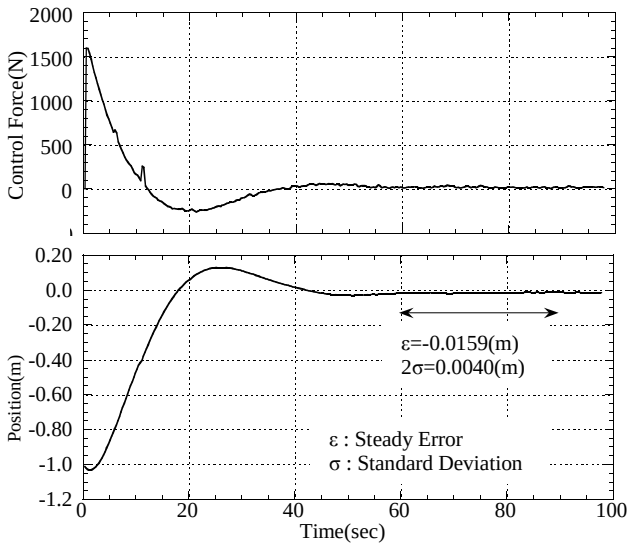

Fig14 Test Results of Optimal Control

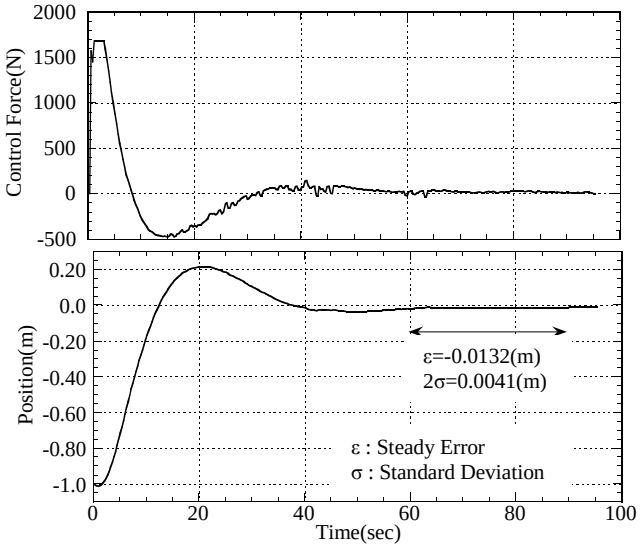

Fig.15 Test Results of Adaptive Control

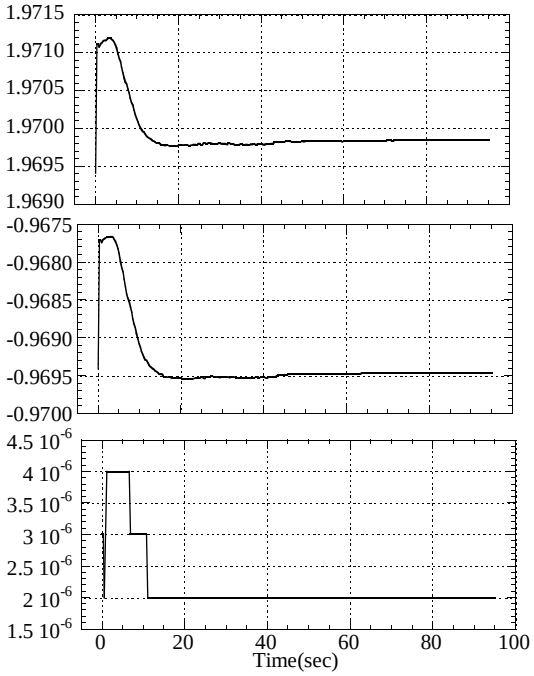

Fig16 Time Series of Estimated θ

The initial transient response in adaptive control was similar to that in optimal control, and this appears to be the direct result of the use of $\boldsymbol{\theta}_0$, $\boldsymbol{R}_0$ and $\boldsymbol{L}_0$ as the initial values.

Fig. 16 shows the time-series of the value of $\boldsymbol{\theta}$ under adaptive control. The fluctuation in the value of $\boldsymbol{\theta}$ observed shortly after the start of control appears to be attributable to the response of the adaptive mechanism to adjust to the changes in the state of the vehicle caused by its motion.

Fig. 17 shows the locus of one of the eigenvalues of the control system of this test. With discrete control, the control system is in the divergent region if the absolute value of the eigenvalue is greater than 1. In this regard, Fig. 17 shows that the estimation mechanism was functioning properly as eigenvalues converged in the stable region.

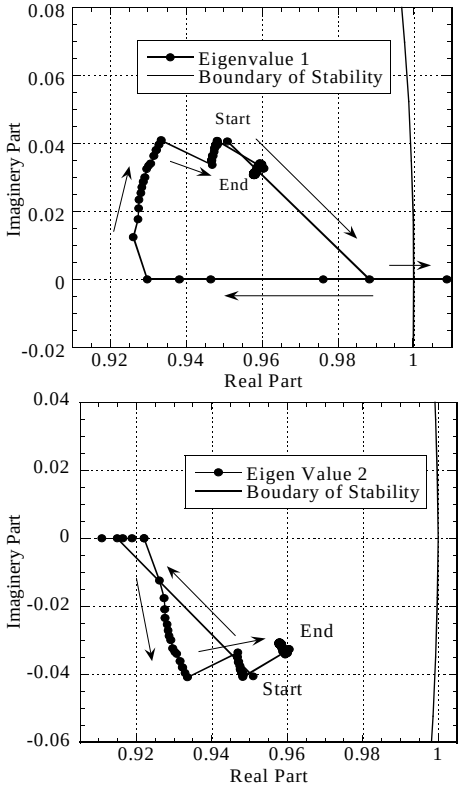

Fig.17 Locus of Eigen Value

VI. CONCLUSION

In this study, ocean field experiments were conducted on the SHINKAI6500 using experimental thrusters as part of research geared towards the improvement of the performance of the propulsion control system. The conclusions are as follows:

(1)The produced experimental thrusters proved to have adequate capabilities in terms of response speed and thrust force.

(2)The surge, sway and yaw drag coefficients of the SHINKAI6500 were measured.

(3)It was learnt that the motion control of the submersible, including position-keeping control, near the ocean bottom can be carried out with sufficiently high accuracy using a combination of experimental thrusters and a Doppler sonar used as a positioning sensor.

(4)Two algorithms, optimal control and Ossman's adaptive control, were used, and both produced excellent results.

REFERENCES

[1] Ossman, K. A., Kamen, E. W., *Adaptive Regulation of MIMO Linear Discrete Time Systems Without Requiring a Persistent Excitation, IEEE Trans.*, Vol. AC-32, No.5, 1987, pp.881-889.

[2] H. Suzuki, T. Shimura, K. Yoshida and N. Oka, *A Basic Research on a Control of Underwater Structure by Adaptive Control, Journal of the Society of Naval Architects of Japan*, Vol. 178 , 1995, pp. 485-494.

[3] Bishop, R. E. D., and Price, W. G., *Hydroelasticity of Ships*, Cambridge University Press